AIP | Journal of Applied Physics

# Numerical investigation of the double-arcing phenomenon in a cutting arc torch

B. R. Mancinelli, F. O. Minotti, L. Prevosto, and H. Kelly

Citation: Journal of Applied Physics **116**, 023301 (2014); doi: 10.1063/1.4887490
View online: http://dx.doi.org/10.1063/1.4887490
View Table of Contents: http://scitation.aip.org/content/aip/journal/jap/116/2?ver=pdfcov
Published by the AIP Publishing



# Numerical investigation of the double-arcing phenomenon in a cutting arc torch

B. R. Mancinelli,[1,a)] F. O. Minotti,[1,2] L. Prevosto,[2] and H. Kelly[1,2]
[1]*Grupo de Descargas Eléctricas, Departamento Ingeniería Electromecánica, Facultad Regional Venado Tuerto (UTN), Laprida 651 (2600) Venado Tuerto (Santa Fe), Argentina*
[2]*Instituto de Física del Plasma (CONICET), Departamento de Física, Facultad de Ciencias Exactas y Naturales (UBA) Ciudad Universitaria Pab. I, (1428) Buenos Aires, Argentina*

(Received 18 April 2014; accepted 26 June 2014; published online 9 July 2014)

A numerical investigation of the double-arcing phenomenon in a cutting arc torch is reported. The dynamics of the double-arcing were simulated by using a two-dimensional model of the gas breakdown development in the space-charge layer contiguous to the nozzle of a cutting arc torch operated with oxygen. The kinetic scheme includes ionization of heavy particles by electron impact, electron attachment, electron detachment, electron–ion recombination, and ion–ion recombination. Complementary measurements during double-arcing phenomena were also conducted. A marked rise of the nozzle voltage was found. The numerical results showed that the dynamics of a cathode spot at the exit of the nozzle inner surface play a key role in the raising of the nozzle voltage, which in turn allows more electrons to return to the wall at the nozzle inlet. The return flow of electrons thus closes the current loop of the double-arcing. The increase in the (floating) nozzle voltage is due to the fact that the increased electron emission at the spot is mainly compensated by the displacement current (the ions do not play a relevant role due to its low-mobility) until that the stationary state is achieved and the electron return flow fully-compensates the electron emission at the spot. A fairly good agreement was found between the model and the experiment for a spot emission current growth rate of the order of $7 \times 10^4$ A/s. © *2014 AIP Publishing LLC*. [http://dx.doi.org/10.1063/1.4887490]

## I. INTRODUCTION

The plasma cutting process is characterized by a transferred electric arc that is established between a cathode, which is a part of the cutting torch, and a work-piece (the metal to be cut) acting as the anode.[1] In order to obtain a high-quality cut, the plasma jet must be as collimated as possible (i.e., it must have high power density). To this end, the transferred arc is constricted by a metallic tube (a nozzle) with a small inner diameter (of the order of 1 mm). A vortex-type high-pressure flow is forced through the nozzle to provide arc stability and to protect its inner wall. The intense convective cooling at the arc fringes due to the vortex flow enhances the power dissipation per unit length of the arc column, which in turn, results in high axis electric field values. Typically, arc voltage drops inside the nozzle of about 50 V or even higher are usually reached.

In the normal mode of torch operation (see Fig. 1(a)), the nozzle is a floating conductor (i.e., it is not electrically connected to any part of the torch circuit). However, since the metallic nozzle itself is at a constant floating voltage, the zero current balance is fulfilled globally along the whole collecting area of the nozzle and not locally (by an ambipolar flux to the nozzle). This means that one part of the nozzle will collect electrons, while the other part will collect ions. Also, due to the fact that the electric current is mainly carried by the electrons, the electron collecting section of the nozzle will be very small as compared with the ion collecting region. Hence, the nozzle floating potential must be close to the arc voltage at the nozzle inlet. In consequence, the voltage drop between the metallic nozzle and the plasma at the nozzle exit reaches a value very close to the total arc voltage drop inside the nozzle.[1] Since this voltage drop is confined within a thin space-charge layer, which separates the plasma from the nozzle, the corresponding electric field strength can be high. Under certain operating conditions (as for instance, a too small gas mass flow), this electric field can be high enough to develop a gas breakdown, and ultimately a secondary discharge current will flow through the floating nozzle, carrying a substantial part of the arc current (see Fig. 1(b)). Such type of arc instability is called double-arcing. A basic feature of the double-arcing phenomenon is that the nozzle behaves both as cathode and anode, and that involves breakdown of a high-temperature gas between one electrode (the nozzle) and a plasma boundary. These features resembles unipolar arc discharges.[2]

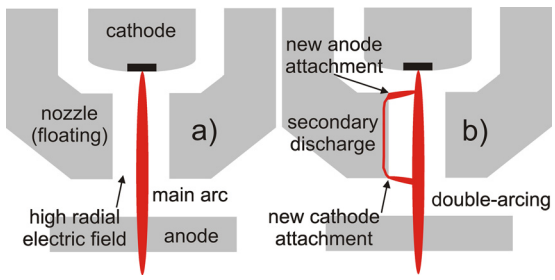


FIG. 1. Normal (a) and double-arcing (b) modes of nozzle operation of a transferred arc cutting torch.

[a)]Electronic mail: bmancinelli@frvt.utn.edu.ar

 

Relatively little has been done to explore and understand the double-arcing phenomenon, especially considering that it is one of the main drawbacks that limit the capabilities of the plasma arc cutting process. The first hypothesis on the mechanism that triggers double-arcing in a cutting torch was formulated by Nemchinsky.[3] In that work, it was suggested that this mechanism consists in a Townsend-like avalanche developing in the cold gas layer that wraps the nozzle's orifice. This mechanism was further considered by Prevosto *et al.*[4–6] Experiments conducted with the nozzle itself as a large-sized Langmuir probe supported the Townsend avalanche hypothesis as the trigger mechanism, but indicated that it is developed in the space-charge layer that separates the plasma and the nozzle, rather than in the cold gas envelope.[4,5] A complementary numerical description of the space-charge layer in conditions suited to Langmuir probe measurements[4] was presented in Ref. 6. The numerical results showed that at the exit of the nozzle the radial electric field value at the nozzle wall could be strong enough to trigger the layer breakdown in conformity with Paschen's law; thus supporting the Townsend-like breakdown as the double-arcing trigger mechanism. Nemchinsky also proposed that non-conducting films, formed from eroded material from the cathode and deposited on the nozzle wall, could also play a triggering role.[7]

Although there are some differences in the conclusions of these works, all concur that double-arcing results from a very high voltage drop inside the nozzle,[1,3–7] however, there is no clear understanding of what is the layer dynamics which ultimately closes the current loop through the nozzle.

In this work, a numerical investigation of the double-arcing phenomenon in a cutting arc torch is reported. The dynamics of the double-arcing are simulated by using a two-dimensional model of the gas breakdown development in the space-charge layer contiguous to the nozzle of a cutting arc torch operated with oxygen. The kinetic scheme includes processes of ionization of heavy particles by electron impact, electron attachment, electron detachment, electron–ion recombination, and ion–ion recombination. Complementary measurements during double-arcing phenomena are also reported. A comparison with the model results is presented.

The paper is organized as follows: The numerical model is described in Sec. II, while the model results and its comparison with the experiment are presented in Sec. III. The conclusions are summarized in Sec. IV.

## II. TWO-DIMENSIONAL FLUID MODEL OF THE SPACE-CHARGE LAYER

### A. Task geometry

As it was shown in previous works,[4–6] the elastic mean-free-paths for all species are much smaller than the space-charge layer thickness and therefore the fluid description applies. Since the layer is collisional, there is no need for an intermediate layer (the pre-layer) and the layer edge coincides with the unperturbed non-local thermal equilibrium (NLTE) high-pressure quasi-neutral plasma.[8] The model geometry showing the collisional space-charge layer contiguous to the floating nozzle is sketched in Fig. 2. Since the layer remains thin as compared with the nozzle orifice radius, a planar geometry is used, in which $x$ and $y$ are the axial and normal to the nozzle coordinates, respectively.

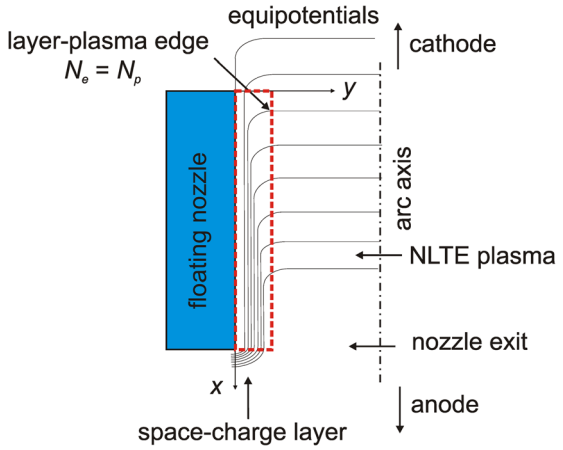


FIG. 2. Schematic of the layer formed between the NLTE plasma and the nozzle wall. The boundaries of the computational domain were marked with a dashed red line.

### B. Main equations of the hydrodynamics approximation

The fluid model is based on the following balance equations for electrons and ions coupled to the Poisson's equation:[9,10]

$$\frac{\partial N_e}{\partial t} + \nabla \cdot \bar{\Gamma}_e = S_{ion} + S_{\det} - S_{rec}^{ei} - S_{att}, \tag{1}$$

$$\frac{\partial N_p}{\partial t} + \nabla \cdot \bar{\Gamma}_p = S_{ion} - S_{rec}^{ei} - S_{rec}^{ii}, \tag{2}$$

$$\frac{\partial N_n}{\partial t} + \nabla \cdot \bar{\Gamma}_n = S_{att} - S_{rec}^{ii} - S_{\det}, \tag{3}$$

$$\nabla^2 V = -\frac{1}{\varepsilon_0}(q_p N_p + q_n N_n + q_e N_e), \tag{4}$$

(here indices $e$, $p$, and $n$, indicate electrons, positive, and negative ions, respectively; $N_\alpha$, $q_\alpha$, and $\bar{\Gamma}_\alpha$ are the particle number density, the particle charge, and the flux density of a species $\alpha$ ($\alpha = e, p, n$); $S_{ion}$, $S_{att}$, $S_{det}$, and $S_{rec}$ are, respectively, the rates of ionization, electron attachment, electron detachment, electron-ion ($ei$) and ion-ion ($ii$) recombination; $V$ and $\varepsilon_0$ are the electrostatic potential and the vacuum permittivity constant, respectively). The particle fluxes in Eqs. (1)–(3) were obtained from the momentum balance equations for each type of particle by using the drift diffusion approximation and neglecting particle inertias and thermal diffusion

$$\bar{\Gamma}_e = -N_e \mu_e \bar{E} - D_e \nabla N_e, \tag{5}$$

$$\bar{\Gamma}_p = N_p \mu_p \bar{E} - D_{pp} \nabla N_p - D_{pn} \nabla N_n, \tag{6}$$

$$\bar{\Gamma}_n = -N_n \mu_n \bar{E} - D_{nn} \nabla N_n - D_{np} \nabla N_p, \tag{7}$$

(here $\mu_\alpha$, $\bar{E}$, and $D_e$ are the mobility of species $\alpha$, the electric field ($\bar{E} = -\nabla V$), and the diffusion coefficient of electrons, respectively; $D_{pp}$, $D_{pn}$, $D_{nn}$, and $D_{np}$ represent coefficients of binary diffusion because there are two types of ions).[11] The

electron mobility and diffusivity were defined, respectively, as $\mu_e \equiv q_e/(m\,\nu_e)$ and $D_e \equiv \mu_e k\,T_e/e$ (here, $m$, $\nu_e$, $k$, and $T_e$ are the electron mass, the electron collision frequency, the Boltzmann's constant, and the electron temperature, respectively). To calculate $\nu_e$, a constant electron temperature of $T_e = 5500$ K was specified in the model, deduced from previous experiments.[4,5] The mobility and binary diffusion coefficients of ions were calculated under the assumption of a perfectly absorbing wall (the ions diffuse to the nozzle wall where they recombine and then diffuse back to the plasma as neutrals).[12]

### C. Kinetic scheme

Pure oxygen was considered. Four oxygen species (molecules ($O_2$), atoms ($O$), positive molecular ions ($O_2^+$), and negative molecular ions ($O_2^-$)) and electrons ($e$) were incorporated to the model. Formation of complex ions (as the conversion of $O_2^+$ into $O_4^+$ and others) was not considered since its concentration is typically low for the considered range of gas temperature (about 1000 K) and also because the ions did not play a relevant role in the dynamics of the discharge. The following reactions were included in the model:

1. Electron ionization

$$e + O_2 \rightarrow e + e + O_2^+, \qquad k_9 = f\left(\frac{E}{N}\right). \tag{8}$$

2. Electron attachment

$$e + O_2 + O_2 \rightarrow O_2^- + O_2, \qquad k_{10} = 1.4\times10^{-41}\left(\frac{300}{T_e}\right)\exp\left(-\frac{600}{T}\right)\times\exp\left(700\frac{T_e - T}{T_e\,T}\right)\mathrm{m^6 s^{-1}}. \tag{9}$$

3. Electron-ion recombination

$$e + O_2^+ \rightarrow O + O, \qquad k_{11} = 2\times10^{-13}\left(\frac{300}{T_e}\right)\mathrm{m^3 s^{-1}}. \tag{10}$$

4. Ion-ion recombination

$$O_2^- + O_2^+ + O_2 \rightarrow O_2 + O_2 + O_2, \qquad k_{12} = 2\times10^{-37}\left(\frac{300}{T}\right)^{5/2}\mathrm{m^6 s^{-1}}. \tag{11}$$

5. Electron detachment

$$O_2^- + O_2 \rightarrow O_2 + O_2 + e, \qquad k_{13} = 2.7\times10^{-16}\left(\frac{T}{300}\right)^{1/2}\times\exp\left(-\frac{5590}{T}\right)\mathrm{m^3 s^{-1}}. \tag{12}$$

(here $k_{10}$–$k_{13}$ are the rate constants taken from Refs. 9 and 13; $E$, $N$, and $T$ are the electric field strength, the neutral particle density, and the heavy particles temperature). The ionization rate constant $k_9$ was calculated by solving the Boltzmann kinetic equation with the help of the BOLSIG software package,[14] the corresponding cross sections being taken from Ref. 15. The photo-ionization was not considered in the model because it did not play a dominant role in the Townsend breakdown. Estimations based on the radiation emitted from the hottest part of the arc (electron temperature about 18 000 K) have showed that the photo-ionization rate is about $10^{26}$ $\mathrm{m^3 s^{-1}}$, which is much lower than that of corresponding to electron impact of about $10^{27}$–$10^{29}$ $\mathrm{m^{-3} s^{-1}}$ in this scenario. The reaction terms of the Eqs. (1)–(3) were then expressed in the following forms: $S_{ion} = k_9\,N_e\,[O_2]$, $S_{\mathrm{det}} = k_{13}\,[O_2^-]\,[O_2]$, $S_{rec}^{ei} = k_{11}\,N_e\,[O_2]$, $S_{rec}^{ii} = k_{12}\,[O_2^-]\,[O_2]\,[O_2^+]$, and $S_{att} = k_{10}\,N_e\,[O_2]\,[O_2]$; where the number density of heavy particles was denoted by square brackets. The number density of atomic oxygen was neglected as compared with the density of the molecules background ($N = [O_2]$). The total pressure ($p$) equation, $p/k = (N + N_p)\,T + N_e\,T_e$, was used to calculates $N$. Since the ion mass is almost equal to that of the neutral gas, the ions are efficiently cooled by the background gas. Thus, the heavy particle's temperature was considered constant in space and time, with a value (used in previous works[4–6]) $T = 1000$ K. Although the actual $T$ value is in principle very hard to obtain, it must be lower than the copper melting temperature (<1400 K), which represents the upper limit of $T$. The impact of the $T$ value on the model results was checked by repeating the calculations with $T = 1400$ K. The changes in the charged particles current densities at the nozzle wall were everywhere less than 30%.

### D. Boundary conditions

The boundary flux for each ion species ($\alpha = n, p$) at the nozzle wall under the drift-diffusion approximation was defined as[16]

$$\bar{\Gamma}_\alpha \cdot \hat{n} = \left[(2\,a_\alpha - 1)\,S_g\,(q_\alpha)\,\mu_\alpha \bar{E}\cdot\hat{n}\,N_\alpha - \frac{1}{2}\,v_{th}\,N_\alpha\right], \tag{13}$$

(here the number $a_\alpha$ is set to one if the drift velocity is directed toward the wall, and zero otherwise, $\hat{n}$ is an outward normal unit vector at the wall and $v_{th}$ is the ion thermal velocity). The electron flux boundary at the nozzle includes also the electron emission from the wall[16]

$$\bar{\Gamma}_e\cdot\hat{n} = \left[\begin{array}{l}(2a_e - 1)S_g\,(q_e)\,\mu_e\bar{E}\cdot\hat{n}N_e - \frac{1}{2}v_{th,e}N_e + \frac{1}{2}v_{th,e}N_{\gamma,em}\\ +2\,(1-a_e)\left(-\gamma\bar{\Gamma}_p + \bar{\Gamma}_{em}\right)\cdot\hat{n}\end{array}\right], \tag{14}$$

(here $v_{th,e}$ is the electron thermal velocity, $N_{\gamma,em}$ is the number density of the electrons emitted from the nozzle wall, $\gamma$ is the average number of electrons emitted per incident ion, and $\bar{\Gamma}_{em}$ is the electron emission from the cathode spot). According to condition (14), only the electrons from the bulk

of the discharge contribute to the diffusive flux toward the wall (so that the emitted electrons do not flow back). The voltage of the floating nozzle ($V_N$) was self-consistently calculated by using the total current (conduction plus displacement) conservation throughout the nozzle surface

$$\oiint_{nozzle\ surface} \left( \sum_{\alpha=e,p,n} q_\alpha \bar{\Gamma}_\alpha + \varepsilon_0 \frac{\partial \bar{E}}{\partial t} \right) \cdot \hat{n}\, dS = 0. \qquad (15)$$

At the arc boundary, axial profiles of plasma and neutral gas densities were specified as constant in time. Since plasma conditions at the nozzle wall are inaccessible to plasma diagnostics if the nozzle is in a floating condition, no experimental verification is possible. However, it is expected that these plasma conditions do not change appreciably because the plasma characteristics at the wall are quite independent of the arc current.[17] Besides, at the arc boundary, the conservation of the particle flux was used for the negative ions. The arc voltage axial profile was varied in time following the experimentally determined variation. At the nozzle inlet and exit, open boundary conditions were assumed (the second normal derivatives of all model variables were set to zero at these surfaces).

### E. Numerical aspects

The fluid model equations were approximated by a finite difference discretization scheme of first-order accuracy in space and time. This method provides a higher computational speed when compared with higher-order schemes, also reducing computational and programming effort, but may introduce numerical viscosity in the solution. However, a comparison between the results obtained by solving convection-diffusion transport equations with this method, and the results obtained using a higher-order scheme showed that within the limits of computational errors, both results coincide.[9] The charged particle densities in the transport term of the balance equations were treated implicitly while the electric field was handled explicitly. The drift-diffusion fluxes in the balance equations were spatially discretized using the exponential difference scheme.[18] The discretized model equations were then solved iteratively by using the strongly-implicit procedure (SIP).[19] A uniform rectangular grid with $10 \times 10$ mesh cells covered the rectangular task geometry. The mesh sizes in $x$ and $y$ directions were 0.45 mm and 0.84 $\mu$m, respectively. The accuracy of the results was checked by repeating them up to a time of 1 $\mu$s with a $20 \times 20$ grid. The change in the nozzle voltage was less than 5%. A temporal step shorter than $5 \times 10^{-13}$ s was used to ensure numerical stability.

### F. Experimental data

The model was validated for a low-current cutting torch with a copper nozzle of 4.5 mm length, with a bore radius of 0.5 mm. A sketch of the torch used is given in Fig. 3. Operating (measured) conditions were arc current, 30 A; oxygen gas flow rate, 2 Nl/min; torch chamber pressure, $p_{ch} = 3.5$ atmospheres; cathode voltage, $V_C = -93$ V,

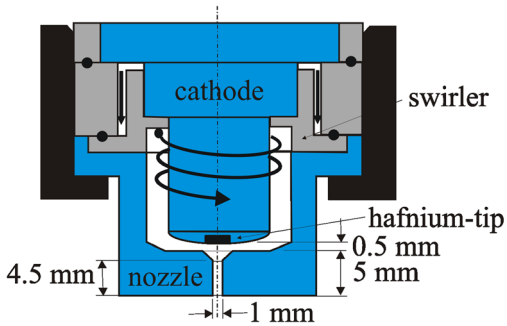


FIG. 3. Scheme of the arc torch indicating several geometric dimensions.

$V_N = -75$ V; and arc voltage at the nozzle exit, $-20$ V (leading to a voltage drop of 55 V across the layer at the nozzle exit). The $V_N$ signal was obtained using a high-impedance voltage-divider (101 k$\Omega$ of total resistance) connected between the nozzle and the anode of the arc. The voltage measurements (with respect to the grounded anode) were performed by using a two-channel oscilloscope (Tektronix TDS 1002 B with a sampling rate of 500 MS/s and an analogical bandwidth of 60 MHz). A floating sweeping electrostatic probe was also used to infer the arc voltage at the nozzle exit.[20,21] The experimental uncertainty in the electric measurements was within $\pm 8\%$.

At the above operating conditions, the arc was highly unstable. Figure 4 shows a typical double-arcing phenomenon. A sudden increment in the nozzle voltage signal around $t = 0$ in the Fig. 4 (with a voltage variation of about 30 V and duration of around 15 ms) indicating a sharp change in the nozzle charge collection is observed. The arc (cathode) voltage waveform resulted quite less perturbed by the double-arcing.

As it is observed in Fig. 4, the arc voltage signal presents an oscillatory component (with a main frequency of 150 Hz, which is the fundamental frequency of the power source ripple) that also modulates the nozzle voltage waveform during the double-arcing phenomenon. This is because the power source ripple has strong influence on the plasma characteristics inside the nozzle.[5] During the experiment, the nozzle was not destroyed after several double-arcing events as showed in Fig. 4. This fact seems to indicate that only a

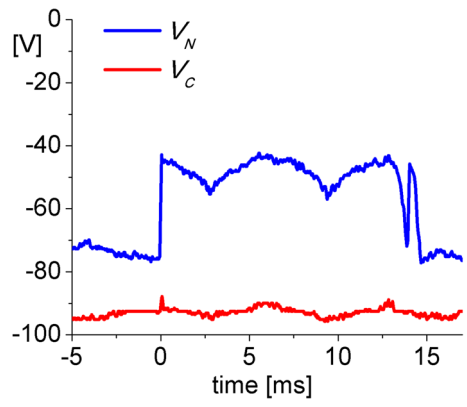


FIG. 4. Typical cathode and nozzle voltage signals during a double-arcing event.

fraction of the main arc current (30 A) circulated throughout the nozzle body.

## III. MODEL RESULTS AND DISCUSSION

Two different simulations were performed. In the first simulation, the stationary distributions of the particles and gas voltage (including the voltage of the floating nozzle) were obtained inside the layer for conditions close to double-arcing. These results were then used as initial conditions for the second simulation in which the double-arcing development was induced by the ignition of a cathode spot at the exit of the nozzle (where the radial electric field exceeds the Townsend's threshold) inner surface.

### A. Initial particle densities and voltage distributions in the layer

The initial model distributions were obtained for a task geometry with 4.5 mm in length and 8.4 $\mu$m in thickness. This thickness corresponded to an estimation based on the Paschen law[22] for the following gas conditions at the nozzle exit: voltage drop = 55 V, $p = 1$ atmosphere, and $T = 1000$ K. The pressure distribution in the gas was assumed as a linearly decreasing function of the axial position, from 3.5 atm at the torch inlet to 1 atm at the nozzle exit. A similar axial variation was assumed for the arc voltage, varying from $-80$ V at the nozzle inlet to $-20$ V at the nozzle exit. The plasma density profile at the arc boundary corresponded to an estimation based on a collisional layer model[23] coupled to a generalized Saha equation.[24] It resulted in an almost linear profile varying from $1.5 \times 10^{18}\,\mathrm{m}^{-3}$ at the nozzle inlet to $1.4 \times 10^{20}\,\mathrm{m}^{-3}$ at the nozzle exit. At the initial time step, a linearly interpolating function for the voltage distribution in the gas was assumed (a value of $-81$ V was set for the nozzle voltage). The initial distribution of the electron density obeyed the Boltzmann distribution with the electric field. The initial positive ion density distribution was assumed decreasing toward the nozzle due to the ions acceleration in agreement with previous results.[6] Initially, the amount of negative ions was assumed negligible everywhere in the gas.

The iterative method continued until the displacement current was negligible as compared with the conduction current at the nozzle wall. The stationary spatial distributions in the layer for conditions close to double-arcing are presented in Fig. 5. As it is observed in Fig. 5(a), the electron density shows a very steep drop near the layer edge except close to the nozzle inlet, where the nozzle voltage is slightly higher than that of the plasma (as shown Fig. 5(d)), with a virtually zero value everywhere inside the layer. From Fig. 5(d), it is also observed that the voltage drop between the metallic nozzle and the plasma at the nozzle exit reaches a value very close to the total arc voltage drop inside the nozzle, giving rise to a local electric field of high magnitude (around $10^7$ V/m), which is near or over the corresponding breakdown threshold value. However, the lack of electrons at the nozzle exit hampers the layer breakdown development. On the other hand, the voltage of the floating nozzle resulted around $-75$ V, in agreement with the experimental value showed in Fig. 4. The positive ion density (given in

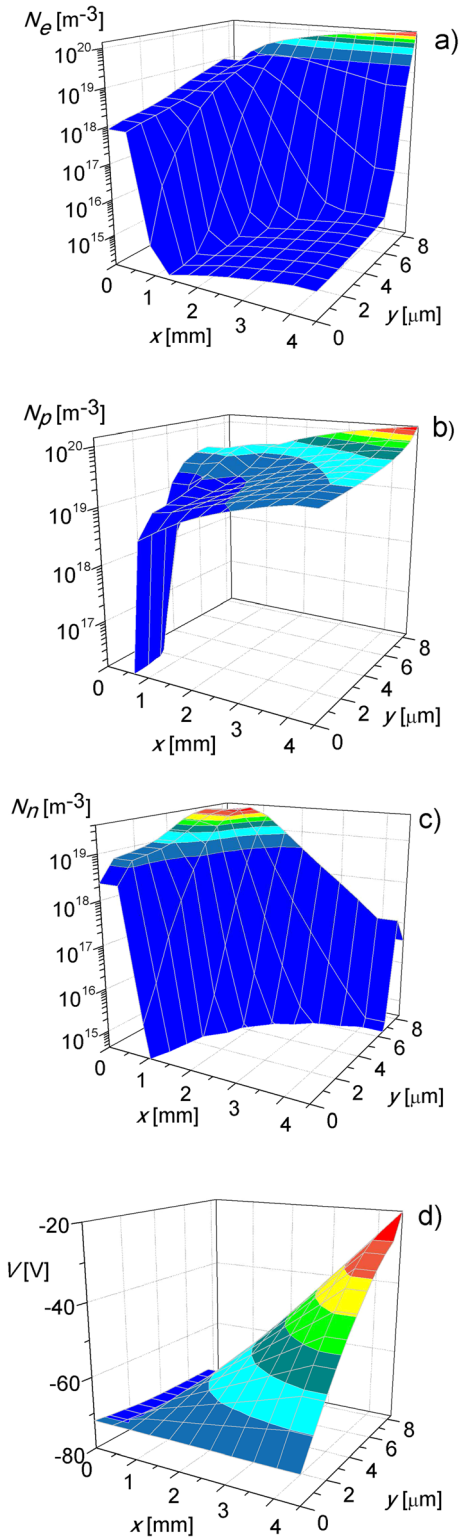


FIG. 5. Numerical particles densities and voltage distributions in the layer in conditions previous to double-arcing: (a) electron density; (b) positive ion density; (c) negative ion density, and (d) gas voltage.

Fig. 5(b)) presents a slow decreasing toward the wall (due to the ion acceleration at an almost constant ion flux) except at the nozzle inlet, where $N_p$ drops sharply near the layer edge due to the repulsive electric field. A relatively high negative ion density is observed close to the nozzle inlet (as showed Fig. 5(c)) due to electron attachment. However, as the

electron density distribution results comparable with that of the negative ions inside the layer, the negative ion current toward the wall resulted negligible as compared with the electron one, consistent with previous experiments (see Fig. 3(a) of Ref. 4).

The ($y$-component) current density axial distributions for electrons and positive ions at the nozzle wall are presented in Fig. 6. It is observed that the electron current is concentrated mostly at the nozzle inlet (where the radial electric field is directed toward the plasma), while the positive ion current density is collected by almost the entire nozzle inner surface. This numerical result confirms that the zero current balance in the nozzle is fulfilled globally along the whole collecting area of the nozzle (and not locally), giving rise to a loop of weak current (of about 0.1 ampere) through the nozzle. A very low electron emission from the nozzle wall into the plasma, due to ion impact for a secondary emission coefficient $\gamma = 0.05$,[22] can be also seen toward the nozzle exit.

### B. Double-arcing dynamics

When the electric field strength in the gas is near or over the electric field threshold to initiate and sustain an arc, there is a strong local emission of electrons into the gas from a cathode spot at the nozzle.[2] Local microscopic protrusions in the nozzle can substantially enhance the applied electric field by an order of magnitude or higher, leading to a local strong thermo-field emission.[22] Also non-conducting films formed from eroded cathode material can also play a role.[7] Thus, a cathode spot will be formed at the exit of the inner nozzle surface in a characteristic time of about $10^{-7}$–$10^{-4}$ s. Since a comprehensive model of the initiation of a cathode spot[25] is beyond the scope of this investigation, an electron emission flux into the plasma was prescribed at the last mesh cell on the nozzle wall. Such an electron emission flux was specified as a linear function of time ($t$), in the form $\bar{\Gamma}_{em} \equiv (d\Gamma_{em}/dt)\, t\, \hat{n}$, where the electron emission flux rate $(d\Gamma_{em}/dt)$ was used as a model parameter to adjust the experimental results. As the only quantity experimentally available was $V_N$, the validation of the model was then restricted to such a quantity.

Three different emission flux rate values were investigated ($d\Gamma_{em}/dt = 2.2 \times 10^{29}$, $3.1 \times 10^{29}$ and $4.0 \times 10^{29}$ m$^{-2}$s$^{-2}$; corresponding to spot emission current growth rates of $dI_{em}/dt = 5 \times 10^4$, $7 \times 10^4$ and $9 \times 10^4$ A/s, respectively). Figure 7 gives the comparison between the model and the experimental data during the short rise-time (around $10^{-4}$ s) of the nozzle voltage increment (which corresponded to the double-arcing development around $t = 0$ in Fig. 4). For $t$ higher than $10^{-4}$ s, a zero value of $dI_{em}/dt$ was specified. A fairly good agreement is observed between the model and the experiment for the investigated values of $dI_{em}/dt$. The formation dynamics of the cathode spot play a key role in the increase in the nozzle voltage, which in turn allows more electrons to return to the wall at the nozzle inlet. The return flow of electrons closes the current loop of the double-arcing. The increase in the (floating) nozzle voltage is expected because the augmented electron emission from the wall into the plasma should be mainly compensated by the displacement current (the ions do not play a relevant role due to its low-mobility) until that the stationary state is achieved and the electron return flow fully compensates the electron emission.

The spatial model distributions for a fully-developed double-arcing ($t > 10^{-4}$ s) corresponding to a spot emission current growth rate of $7 \times 10^4$ A/s are presented in Fig. 8. Figure 9 presents the corresponding ($y$-component) electron and positive ion density currents at the nozzle wall.

The spatial distribution of the electron density (showed in Fig. 8(a)) presents large differences with respect to distribution of Fig. 5(a). In particular, high electron density values are observed close to the wall at the nozzle exit, related to the electron emission from the cathode spot, and also at the nozzle inlet, where the electrons flow into the nozzle. Such a high electron density at the wall leads also to an increased electron thermal conductivity, thus enhancing the thermal conduction flux to the wall. Furthermore, the rise in the electron density at the wall produced ionization events, thus resulting in an increase in the positive ion density. This is particularly obvious at the nozzle exit and also at the inlet (as shown Fig. 8(b)) because of the enhancement of the local electric field strength due to the redistribution of the gas

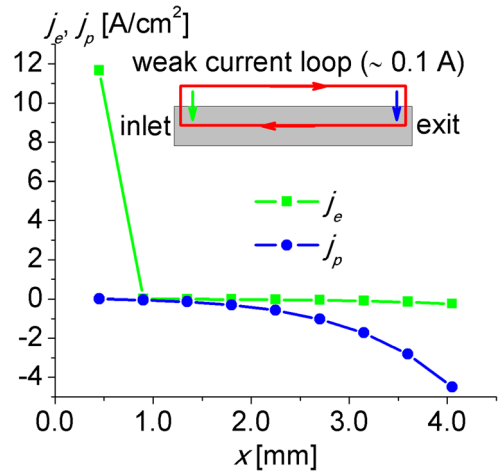


FIG. 6. Axial distributions of the electron and positive ion current densities at the nozzle wall. A sketch of the weak current loop throughout the nozzle is given at the inset.

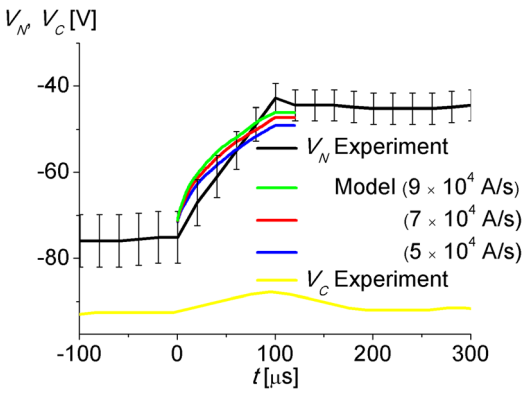


FIG. 7. Comparison between the model and the experiment for the investigated values of the spot emission current growth rate. The theoretical results are shown for $t \leq 1.2 \times 10^{-4}$ s.

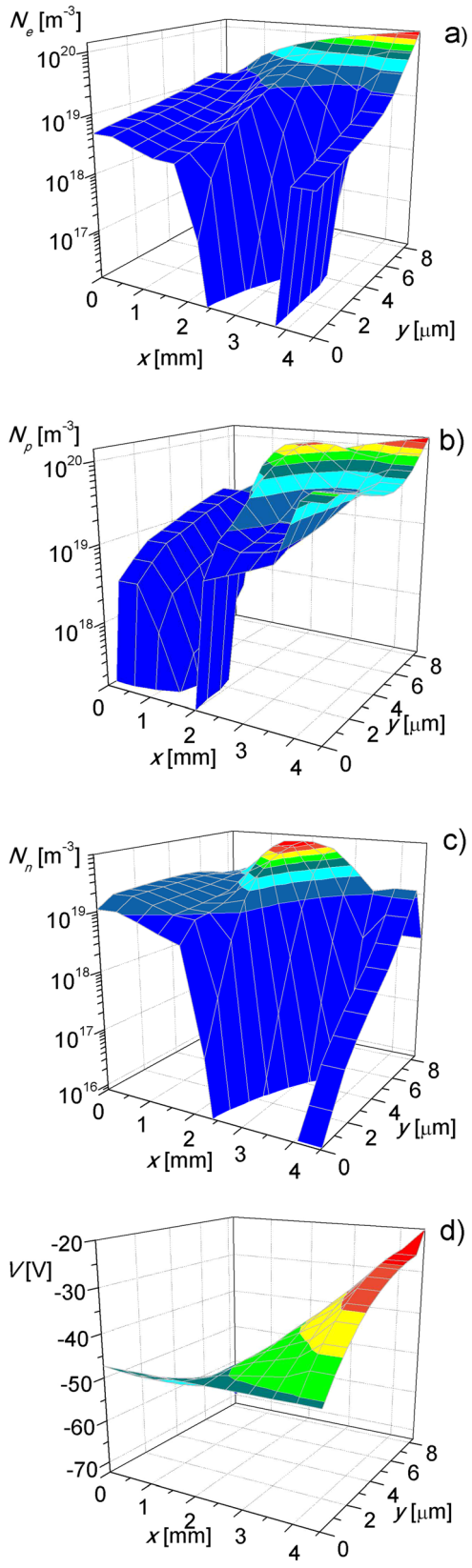


FIG. 8. Numerical particles densities and voltage distributions in the layer for a fully-developed double-arcing: (a) electron density; (b) positive ion density; (c) negative ion density, and (d) gas voltage.

voltage (showed in Fig. 8(d)). The negative ion density distribution (showed in Fig. 8(c)) approximately follows the electron density distribution (owing to the electron attachment reaction), except close to the wall at the nozzle exit due to the repulsive field.

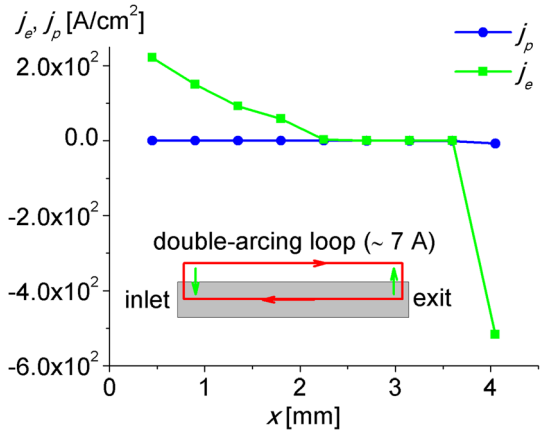


FIG. 9. Axial distributions of the electron and positive ion current densities at the nozzle wall for a fully-developed double arcing (spot emission current growth rate of $7 \times 10^4$ A/s). A sketch of the double-arcing current loop throughout the nozzle is given at the inset.

As it is observed from Figure 9, the current at the nozzle wall for a fully-developed double arcing is mainly transported by electrons (the positive ion contribution at the nozzle exit is less than 5% of the total current), giving rise to a current loop of about 7 A in this case (spot emission current growth rate of $7 \times 10^4$ A/s), which represents an appreciable fraction of the main arc current, but apparently insufficient to destroy the nozzle, according to the experimental observations.

It is important to stress that the current loop of the double-arcing (few amperes) requires the existence of a strong local electron emission from the nozzle wall into the plasma, which cannot be provided by ion impact (even considering an unrealistic high $\gamma$ coefficient) or by photon impact (previous estimates in this kind of cutting torches showed that the photoemission from the nozzle yields a maximum electron current of 2.5 mA).[4] Hence, such a high-electron emission can be only provided in this scenario by a cathode spot (thermo-field emission).[22]

## IV. CONCLUSIONS

The dynamics of the double-arcing in a low-current cutting arc torch were numerically investigated. Complementary measurements during double-arcing phenomena were also conducted. A marked rise of the nozzle voltage was found. The numerical results showed that the dynamics of a cathode spot at the exit of the nozzle inner surface play a key role in the growth of the nozzle voltage, which in turn leads more electrons to return to the wall at the nozzle inlet. The return flow of electrons closes the current loop of the double-arcing. The rise of the (floating) nozzle voltage is due to the increase in the spot electron emission, which is compensated mainly by the displacement current until the stationary state is achieved and the electron return flow fully compensates the electron emission. A fairly good agreement was found between the model and the experiment for a spot emission current growth rate of the order of $7 \times 10^4$ A/s.

## ACKNOWLEDGMENTS

This work was supported by grants from the CONICET (PIP 11220090100219) and Universidad Tecnológica Nacional (PID-UTN 1389). F.O.M., H.K., and L.P. are members of the CONICET.

[1]V. A. Nemchinsky and W. S. Severance, J. Phys. D: Appl. Phys. **39**, R423 (2006).
[2]H. J. G. Gielen and D. C. Schram, IEEE Trans. Plasma Sci. **18**, 127 (1990).
[3]V. A. Nemchinsky, J. Phys. D: Appl. Phys. **31**, 3102 (1998).
[4]L. Prevosto, H. Kelly, and B. Mancinelli, J. Appl. Phys. **105**, 013309 (2009).
[5]L. Prevosto, H. Kelly, and B. Mancinelli, J. Appl. Phys. **110**, 083302 (2011).
[6]L. Prevosto, H. Kelly, and B. Mancinelli, J. Appl. Phys. **105**, 123303 (2009).
[7]V. A. Nemchinsky, J. Phys. D: Appl. Phys. **42**, 205209 (2009).
[8]R. N. Franklin, J. Phys. D: Appl. Phys. **36**, R309 (2003).
[9]S. V. Pancheshnyi and A. Yu. Starikovskii, J. Phys. D: Appl. Phys. **36**, 2683 (2003).
[10]R. Veerasingam, R. B. Campbell, and R. T. McGrath, Plasma Sources Sci. Technol. **6**, 157 (1997).
[11]A. B. Murphy, J. Phys. D: Appl. Phys. **29**, 1922 (1996).
[12]M. S. Benilov, J. Phys. D: Appl. Phys. **28**, 286 (1995).
[13]I. A. Kossyi, A. Yu. Kostinsky, A. A. Matveyev, and V. P. Silakov, Plasma Sources Sci. Technol. **1**, 207 (1992).
[14]G. J. M. Hagelaar and L. C. Pitchford, Plasma Sources Sci. Technol. **14**, 722 (2005).
[15]A. V. Phelps and L. C. Pitchford, Phys. Rev. A **31**, 2932 (1985).
[16]G. J. M. Hagelaar, Ph.D. thesis, Technische Universiteit, Eindhoven, 2000.
[17]E. Leveroni and E. Pfender, Rev. Sci. Instrum. **60**, 3744 (1989).
[18]D. L. Scharfetter and H. K. Gummel, IEEE Trans. Electron Devices **16**, 64 (1969).
[19]H. L. Stone, SIAM J. Numer. Anal. **5**, 530 (1968).
[20]L. Prevosto, H. Kelly, and B. Mancinelli, IEEE Trans. Plasma Sci. **36**, 263 (2008).
[21]L. Prevosto, H. Kelly, and F. O. Minotti, IEEE Trans. Plasma Sci. **36**, 271 (2008).
[22]Y. P. Raizer, *Gas Discharge Physics* (Springer, Berlin, Germany, 1991).
[23]T. E. Sheridan and J. Goree, Phys. Fluids B **3**, 2796 (1991).
[24]M. C. M. van de Sanden, P. P. J. M. Schram, A. G. Peeters, J. A. M. van der Mullen, and G. M. W. Kroesen, Phys. Rev. A **40**, 5273 (1989).
[25]P. G. C. Almeida, M. S. Benilov, and M. D. Cunha, IEEE Trans. Plasma Sci. **36**, 1032 (2008).